Title

Trask Loss Enhances Tumorigenic Growth by Liberating Integrin Signaling and Growth Factor Receptor Cross-Talk in Unanchored Cells

Journal

Cancer Research, 73(3)

ISSN

0008-5472

Authors

Spassov, Danislav S
Wong, Ching Hang
Wong, Sunny Y
et al.

Publication Date

2013-02-01

DOI

10.1158/0008-5472.can-12-2496

Peer reviewed

Published in final edited form as:
Cancer Res. 2013 February 1; 73(3): 1168–1179. doi:10.1158/0008-5472.CAN-12-2496.

Trask loss enhances tumorigenic growth by liberating integrin signaling and growth factor receptor cross-talk in unanchored cells

Danislav S. Spassov[1], **Ching Hang Wong**[1], **Sunny Y. Wong**[3], **Jeremy F. Reiter**[2], and **Mark M. Moasser**[1]

[1]Department of Medicine and Helen Diller Family Comprehensive Cancer Center, University of California, San Francisco, San Francisco, CA 94143

[2]Department of Biochemistry and Biophysics and Cardiovascular Research Institute, University of California, San Francisco, San Francisco, CA 94143

[3]Department of Dermatology, University of Michigan, Ann Arbor, MI

Abstract

The cell surface glycoprotein Trask/CDCP1 is phosphorylated during anchorage loss in epithelial cells where it inhibits integrin clustering, outside-in signaling and cell adhesion. Its role in cancer has been difficult to understand, because of the lack of a discernible pattern in its various alterations in cancer cells. To address this issue, we generated mice lacking Trask function. Mammary tumors driven by the PyMT oncogene and skin tumors driven by the SmoM2 oncogene arose with accelerated kinetics in Trask deficient mice, establishing a tumor suppressing function for this gene. Mechanistic investigations in mammary tumor cell lines derived from wildtype or Trask-deficient mice revealed a derepression of integrin signaling and an enhancement of integrin-growth factor receptor crosstalk, specifically in unanchored cell states. A similar restrictive link between anchorage and growth in untransformed epithelial cells was observed and disrupted by elimination of Trask. Together our results establish a tumor suppressing function in Trask that restricts epithelial cell growth to the anchored state.

Keywords

Trask; CDCP1; SIMA135; Src; integrin

Introduction

Epithelial tumor growth is dependent on a number of cellular processes, one of which is cell adhesion. The relationship between tumor growth and cell adhesion is a complicated one. While the normal epithelium is anchored on an underlying basement membrane, epithelial tumors grow without the requirement for anchorage, and free of the boundaries and restrictions associated with basement membranes. Although the loss of anchorage can have a liberating effect, allowing the often erratic and invasive growth of tumors, the absence of cell adhesion can also have a restrictive effect, disabling signaling pathways important in promoting growth, and removing mechanisms that enable cell migration and invasion. In

Corresponding Author Contact: Mark M. Moasser, mark.moasser@ucsf.edu.

Conflicts of interest:
The authors have no conflicts to disclose

particular, adhesion signaling through integrin receptors is known to be important in promoting many aspects of tumor growth including proliferation, survival, migration, invasion, and metastasis (1, 2). Integrins not only mediate the migratory functions of tumor cells, but more specifically, cross-talk between integrins and growth factor receptors is thought to be critically important for some tumors (3–5), particularly those driven by oncogenic growth factor receptors such as HER2/Neu, and in fact the development of HER2/Neu-driven tumors is considerably delayed or suppressed in mice lacking β1 or β4 integrins (6, 7). Therefore the relationship between tumorigenesis and cell adhesion is a complex one that likely involves reconciling the tumor promoting and suppressing consequences of integrin engagement and activation. While integrin signaling is generally linked with cell adhesion, their relationship is subject to layers of regulation, and potentially corruptible in tumors seeking freedom from anchorage but persistency in integrin signaling. Here we describe a Src-driven anti-adhesive pathway that negatively regulates integrin signaling and cell growth during anchorage deprivation, conferring a tumor suppressive role and accounting for its observed decrease or loss of expression in some tumors.

Trask (Transmembrane and Associated with Src Kinases, aka CDCP1, SIMA135, gp140) was independently identified by several groups in the recent decade, studying different aspects of cancer biology (8–11). The Trask protein is a 140kD transmembrane glycoprotein with a large extracellular domain (ECD) containing CUB domains, and a smaller intracellular domain (ICD) containing five tyrosines and a proline-rich region. Trask is proteolytically cleaved within its ECD by serine proteases including MT-SP1 and is expressed in most cells as a blend of 140kD (uncleaved) and 80kD (cleaved) forms in varying ratios (9, 12). Trask is widely and abundantly expressed throughout epithelial tissues and specific hematopoietic cells, but its expression is not readily detected in mesenchymal tissues (13, 14).

In cultured cells we found that Trask undergoes phosphorylation by Src kinases immediately upon the loss of anchorage, and accounts for the majority of cellular phosphotyrosine content in the unanchored state in many cells, and remains phosphorylated until anchorage is restored (13, 15). When phosphorylated, Trask functions to negatively regulate cell adhesion. This is accompanied by its association with β1-integrin complexes, interfering with integrin clustering, and preventing downstream signaling including the phosphorylation of FAK, establishing pY-Trask as a negative regulator of FAK (16). The anti-adhesive effects of phosphorylated Trask are mediated specifically through the inhibition of integrin clustering without an effect on integrin affinity state (16). Consistent with its anti-adhesive functions, Trask knockdown confers increased cell adhesiveness, and constitutive Trask phosphorylation blocks cell adhesion (9, 16, 17). P-Trask interferes with most integrin complexes and adhesion to most matrix ligands, resulting in the inhibition of physical cell-matrix adhesion and consequently the disruption of focal adhesions and focal adhesion signaling through FAK, 130Cas, paxillin, and other focal adhesion proteins (16). Importantly the phosphorylation of Trask and the phosphorylation of focal adhesion proteins, including FAK, occur in exclusion of eachother, defining a phosphotyrosine switch that underlies cell anchorage state (15, 16).

In a survey of human epithelial tumors of different types, we found that Trask is phosphorylated in many tumors, usually in a patchy distribution, including pre-invasive, invasive, and metastatic tumors (18). The phosphorylation of Trask is never seen in normal epithelial tissues except for occasional mitotic or detached cells, consistent with the fully anchored state of the normal epithelium (18). The observed phosphorylation of Trask in tumors may be either a physiological event reflecting the loss of cell anchorage in regions of tumors, or may be a tumor-promoting pathologic event, perhaps due to the activation of Src kinases. Experimental studies using human cancer cell lines fail to support a tumor

promoting function, and in fact suggest a tumor-suppressing function (19). Consistent with a tumor-suppressing function, the expression of Trask is reduced or lost in some tumors compared with the normal epithelia and reduced or absent in some cancer cell lines (19).

In the current study, we set out to more definitively determine the functions of Trask in tumorigenesis. We generated mice lacking Trask function and studied its effects on the development and progression of two oncogene-induced tumors. We found that the loss of Trask significantly accelerates tumorigenesis, confirming a tumor suppressing function. Mechanistic studies on these tumor cells and untransformed epithelial cells reveal that Trask phosphorylation is a mechanism that restricts growth in the unanchored state, at least partly through the inhibition of integrin signaling and its associated cross-talk with growth factor receptors.

Materials and Methods

Targeting vector construction and generation of Trask deficient mice

DNA was amplified from mouse 129 isogenic genomic DNA with Pfu Ultra HF polymerase (Invitrogen). 3 DNA fragments were amplified-A, B, and C. Fragment A was amplified with primers ABF3 5′ AGGCGCTGGACTCCCAGC and AR1 5′ GGCAAGCCAGATTTCAGCCCAA. Fragment B was amplified with primers BF1 5′ ATCCACGAGGTCCCAGACCATC and ABR1 5′ CCTAAGGCTTGTTCCGCGCGC. Fragment C was amplified with primers CF1 5′ CGAGGACGTTCTCCAGGCAGCAC and C20878R 5′ CCTTGGCCAGCTTCCAGGTATG. Fragment B is 1,477 bp long and contains exon 1 of Trask and upstream promoter sequences. Loxp sites were engineered at the flanks of fragments B and restriction sites EcoRV, SacI and Swa-1 were introduced immediately adjust to the loxp sites for diagnostic purposes. Fragment A is 3 kb long and serve as 5′ arm of the vector, fragment C is 8.5 kb long and serve as a 3′ arm. The fragment A, B and C were cloned into pB6 vector. In this vector the Neo cassette is flanked by FRT sites, and the expression of Neo is driven by RNA-pol II promoter. The entire sequence of the targeting vector was determined and found to be correct; and no additional mutations resulting from PCR amplification were found. The targeting construct was linearized with ScaI and electroporated into 129 ES cells. Genomic DNA isolated from 500 G418 resistant ES cell colonies was analyzed by Southern blotting. Several correctly targeted ES cell clones were identified and injected into blastocysts to generate chimeric mice. Chimeras were mated with actin-FLP females on C57/BL6 background (Jackson Lab). Germline transmission and Neo excision were confirmed by Southern analysis. The floxed mice were bred for several generations with normal C57/BL6 mice and later mated with EIIa-cre mice (Jackson lab). Excision of fragment B and generation of Trask heterozygous mice was confirmed by PCR. These mice were mated several times with normal C57BL/6 mice and the EIIa-cre transgene was bred out. Trask heterozygous mice were bred to generate $Trask^{+/+}$, $Trask^{+/-}$ and $Trask^{-/-}$ animals for subsequent analysis. Trask heterozygous mice were bred for six consequent generations with normal FVB/N mice before mated with MMTV-PyMT mice. The experiments with K14-Cre^{ERT} SmoM2 mice were performed on a mixed 129/SVJae- C57/BL6 background as previously reported (20).

PCR and Southern blot analyses

Genotyping of floxed mice was performed with Primer 2 (SeqNeo1) 5′-CGCTCAGGCACGTGGGAGAG and Primer 3 (ABR3) 5′-GTGTGGAGTGGGCCCGAAG. Genotyping of Trask $^{+/+,}$ Trask $^{+/-}$ and Trask $^{-/-}$ mice were done by multiplex PCR with three primers- Primer1 (FloxpEcoRV) 5′-TGACTGATACTGGGGCATGGGC, Primer 2 (SeqNeo1) 5′-CGCTCAGGCACGTGGGAGAG and Primer 3 (ABR3) 5′

GTGTGGAGTGGGCCCGAAG. The 5′ external probe was amplified with primers 5F6472-5′-ACTTGTGCCCATCCTGCCTGTG and 5R7894-5′-GCCAACTGCTCCTCCTACCTGC subcloned and sequence confirmed. The 3′ external probe was amplified from mouse genomic DNA with primers F20923 -5′-AGCAGGTCCCTCCATTGCTCAG and R21392- 5′-AGGAATCCAAGGGCCAGCCAG subcloned and sequence confirmed. A 556 bp BamHI SphI fragment was excised from the coding sequence of the Neo cassette and used as a Neo probe. Primes used for genotyping PYMT alleles were PYMT F 5′ GGAAGCAAGTACTTCACAAGGG and PYMT R 5′ GGAAAGTCACTAGGAGCAGGG. Primers used for genotyping SmoM2 were Smo F 5′ TCCTTGAAGAAGATGGTGCG and Smo R 5′ AAGTTCATCTGCACCACCG. Detecting K14-Cre^{ERT} was done with primers CreF 5′ ATACCGGAGATCATGCAAGC CreR 5′ AGGTGGACCTGATCATGGAG.

Animal studies

All animal work was conducted under the guidelines of the UCSF Institutional Animal Care and Use Committee under an IACUC-approved protocol. MMTV-PyMT mice were purchased from Jackson Laboratory. At 12 weeks of age female mice were sacrificed and all mammary tumors were carefully excised, weighted, and photographed. Portions of the tumors were also frozen in liquid nitrogen or fixed in formalin. For histology analysis, mouse tissues were fixed in 10% buffered formalin for 24 hrs and embedded in paraffin. Sections were stained with hematoxolyn and eosin (H&E). For detection of lung metastasis, lungs of Trask wt and null mice were analyzed in H&E sections. K14-Cre^{ERT} and SmoM2 transgenic mice were from J. Reiter lab (UCSF). For induction of Cre recombinase, 30 day old mice were injected intraperitoneally with tamoxifen (T5648, Sigma-Aldrich) dissolved in corn oil (Sigma-Aldrich), at a dose 1 mg for 20 g body weight for 5 consequent days. Skin samples were collected 12 weeks after tamoxifen treatment.

Wound healing was studied following the experimental induction of a skin wound as has been described previously (21, 22). Mice were anesthesized, the dorsal skin was shaved, and a thin 7–8mm long full thickness skin cut was made and allowed to heal naturally. At the indicated early or late timepoints after wounding, mice were euthanized, the wounded skin region excised, fixed, embedded in paraffin, and sections stained as indicated.

Cell culture and immunoblotting

For derivation of cell lines PYMT tumors were cut into small pieces and cultured in Dulbecco's modified Eagle's medium (DMEM)–10% fetal bovine serum (FBS) supplemented with 20 ng/ml epidermal growth factor (Invitrogen). To force cells into suspension, cells were washed in phosphate-buffered saline (PBS), exposed to a 2 mM solution of EDTA in Hank's buffer, and when fully detached cells were span down, resuspended in fresh media and cultured in ULC plates (Corning) for 2 h. ULC plates are not permissive to cell adhesion. For heregulin (HO786, Sigma-Aldrich) stimulation cells were serum and EGF starved overnight, and next day incubated with 10 ng/ml heregulin in serum-free media for 10 min. Cells were incubated with 1μM FAK inhibitor PF562271 (Synmedchem) or 10 μg/ml anti-integrin β1 antibody Ha2/5 (BD Pharmingen) in suspension where indicated.

Total cellular lysates were harvested in modified radioimmunoprecipitation assay (RIPA) buffer (10 mM Na phosphate [pH 7.2], 150 mM NaCl, 0.1% SDS,1% NP-40, 1% Na deoxycholate, protease inhibitors, 1 mM sodium orthovanadate). Tumor lysates were prepared after tumors were quickly frozen in liquid nitrogen, crushed with a mortar and lysed in RIPA buffer. For Western blotting, 50 μg of each lysate was separated by SDS-PAGE, transferred to membrane, and immunoblotted using appropriate primary and

secondary antibodies and enhanced chemiluminescence visualization. For immunoprecipitation studies, 300 μg of lysate was incubated overnight with specific antibodies, immune complexes were collected by protein G-Sepharose beads and washed, and the denatured complexes were immunoblotted as described above. Antiphosphotyrosine antibodies (PY99), anti-FAK, anti-HER2, and anti-HER3 antibodies were from Santa Cruz Biotechnology (Santa Cruz, CA). Anti-phospho-[Y1248] HER2 antibodies antibodies were from Cell Signaling. Anti-phospho-[T202/Y204]-MAPK antibodies and anti-p-[S473]-Akt antibodies were from Cell Signaling.

Sphere formation assay

For sphere formation assay MCF10A cells were seeded in ultra-low attachment plates (6 well clusters) at 10,000 cells/well in 5 mls of full-growth medium. Trask$^{+/+}$ and Trask$^{-/-}$ PyMT cell lines were similarly incubated in ultra-low attachment plates, but in DMEM: F12 medium, containing 10% FBS and 20 ng/ml EGF. The number of spheres was enumerated after 6 days for MCF10A cells and after 7 days for PyMT cell lines. Spheroids counted consisted of approximately 50 cells or more. The MTT assays was performed by addition of 1.5ml 1mg/ml solution of Thiazolyl Blue Tetrazolium Bromide (MTT) (Sigma-Aldrich) in PBS to 5 ml medium containing spheres directly into ultra-low attachment wells. Cells were incubated for two hours, spun down and resuspended in 200 μl DMSO. Absorbance was read in 96 wells plates at 570 nm.

Matrigel growth assays

Three-dimensional (3D) cultures of MCF-10A cells were prepared as described (23). Briefly, 24-well culture plate was first coated with growth factor-reduced Matrigel Matrix (BD Biosciences, MA), followed by an overlay of MCF-10A cells (12.5×103/well) in a 5% Matrigel/media suspension. Cells were grown in a 5% CO2 humidified incubator at 37°C and fed with fully-supplemented MCF-10A media containing 2% Matrigel every 4 days. Cultures were harvested on day 3, 7 and 12 and stained with antibodies against Trask (1:1000), phospho-Trask (1:160) and human laminin V (1:250, MAB19562X, Millipore, CA). Staining was examined and images were acquired by Zeiss LSM 510 NLO Meta confocal microscope.

Generation of Trask knockdown cells

Small hairpin RNA (shRNA) sequences were cloned into pSico-RNeo lentiviral vectors containing a neomycin resistance cassette. For the shTrask-1 construct, the oligonucleotide 5′-TGAATGTTGCTTTCTCGTGGCAGTTCAAGAGACTGCCA-CGAGAAAGCAACATTTTTTTTGGATCC-3′ was annealed to 5′-TCGAGGATCCAAAAAAAATGTTGCTTTCTCGTGGCAGTCTCTTGAACTGCCACG-AGAAAGCAACATTCA-3′ and cloned into HpaI and XhoI sites of the pSicoRNeo vector. To create the shTrask-2 construct, the oligonucleotide 5′-TGATAGATGAGCGGTTTGCAATGCTGATTCAAG-AGATCAGCATTGCAAACCGCTCATCTATTTTTTTTGGCGCGCC-3′ was annealed to 5′-TCGAGGCG-CGCCAAAAAAAATAGATGAGCGGTTTGCAATGCTGATCTCTTGAATCAGCATTG CAAACCGCTCATCT ATCA-3′ and cloned into HpaI and XhoI sites of the vector. For generation of the nonsilencing construct, the oligonucleotides 5′-TGTCTCGCTTGGGCGAGAGTAAGTTCAAGAGACTTACTCTC-GCCCAAGCGAGATTTTTTTGGCGCGCC-3′ and 5′-TCGAGGCGCGCCAAAAAAATCTCGCTTGGGC-GAGAGTAAGTCTCTTGAACTTACTCTCGCCCAAGCGAGACA-3′ were similarly annealed and cloned. The shRNA constructs were transfected into 293T cells along with the appropriate packaging vectors. The resulting lentiviral particles were used to infect

MCF10A cells. Cells were selected with G418 (400 μg/ml), and Trask knockdown was confirmed by Western blotting.

Results

Generation of Trask null mice

A 1.4kb region including exon 1 and regulatory regions of Trask/CDCP1 was flanked by loxP sites (figure 1A) and the germline transmission of this floxed allele was confirmed by Southern analysis of tail genomic DNA (figure 1B) and a PCR assay established for rapid genotyping (figure 1C). Trask$^{fl/+}$ mice on a C57/BL6 background were bred with EIIa-cre mice to generate mice with a null Trask allele. Trask$^{+/-}$ mice were interbred producing Trask $^{+/+}$, Trask$^{+/-}$ and Trask$^{-/-}$ progeny in the predicted Mendelian ratio, suggesting that Trask is not essential for mouse development. The generation of heterozygous and homozygous Trask-null alleles was confirmed by PCR (fig. 1D) and by western blotting (fig. 1E). Trask$^{+/-}$ and Trask$^{-/-}$ mice did not exhibit gross morphological or behavioral abnormalities compared to wild-type mice and histological examination of multiple organ systems found no significant pathology and no observed histological differences.

Tumorigenesis in Trask null mice

MMTV-PyMT mice develop mammary tumors characterized by activation of Src kinases (24) and fairly extensive phosphorylation of Trask (18). Trask$^{+/-}$ mice, backcrossed for 6 generations in the FVB/N background, were bred with MMTV-PyMT transgenic mice in the FVB/N background and subsequent matings undertaken to generate sufficient numbers of female mice carrying the MMTV-PyMT transgene in either of three Trask genotypic backgrounds (Trask$^{+/+}$, Trask$^{+/-}$, Trask$^{-/-}$). PyMT Trask$^{-/-}$ mice showed significantly accelerated tumorigenesis in comparison with PyMT Trask$^{+/+}$ mice (figure 2A). The PyMT Trask$^{-/-}$ mice had to be euthanized at 12 weeks of age because of the presence of numerous large tumors (figures 2B, 2C). In comparison with the PyMT Trask$^{+/+}$ of the same age, the 12-week old PyMT Trask$^{-/-}$ mice had on average 2.6 fold increase in the number of tumors per mouse ($p<0.001$) with an average of 5.7 fold increase in the total tumor burden ($p<0.001$) (figure 2A). The PyMT Trask$^{+/-}$ mice showed a slight, but statistically significant increase in tumorigenesis in comparison with PyMT Trask$^{+/+}$ mice. Lung metastases were present in both arms (supplementary figure S1), but a comparative analysis was not possible as the frequency was low due to the 12-week study termination compelled by the rapid primary tumor growth.

We examined the expression and phosphorylation of Trask in the normal mammary gland and mammary tumors derived from MMTV-PyMT mice. Trask is not phosphorylated in the normal mammary gland consistent with the fully anchored state of the normal epithelium, but its phosphorylation is induced in PyMT tumors (figure 2D, lane 2), consistent with the anchorage-free state in at least some regions of these tumors. The normal mammary gland expresses predominantly the 140kD uncleaved form of Trask, while there is considerable cleavage of Trask and expression of both 140kD and 80kD forms of Trask in the PyMT tumors (figure 2D), likely reflecting enhanced protease activity in the tumor microenvironment. Tumor lysates derived from Trask null mice have no detectable expression of Trask protein (figure 2D, lane 3).

In a second model of tumorigenesis, we studied the development of hyperplasia and tumors in mouse skin driven by a conditional oncogenic Smoothened allele. In SmoM2^{cond}, K14-Cre^{ERT} bitransgenic mice, treatment with tamoxifen induces Cre recombinase activity in the epidermis, leading to activation of the conditional SmoM2 allele and the development of widespread epidermal hyperplasia and neoplasia with complete penetrance (20). These

neoplastic lesions also have elevated activity of Src kinases (supplementary figure S2). To study the function of Trask in this type of tumor, we bred Trask$^{+/-}$ mice (3 generations of backcrossing in the C57/BL6 background since gene targeting) with K14-Cre^{ERT} and SmoM2^{cond} mice in the C57/BL6 background to generate Trask$^{+/-}$ SmoM2^{cond} K14-Cre^{ERT} mice and bred them with Trask$^{+/-}$ mice. From among the progeny, we selected Trask$^{+/+}$ SmoM2^{cond} K14-Cre^{ERT} and Trask$^{-/-}$ SmoM2^{cond} K14-Cre^{ERT} mice for tamoxifen treatment. Tamoxifen treatment of these mice resulted in the development of hyperplastic skin disease of the ear and tail as previously reported (20). The phenotype of the epidermal disease was significantly more severe in Trask$^{-/-}$ mice compared with Trask$^{+/+}$ mice. In Trask$^{-/-}$ mice the skin became much more thick and more widespread, with gross changes including hair loss and scaling, particularly evident on the abdominal skin (figure 3A). These mice developed hunched postures and had to be euthanized 12 weeks after tamoxifen treatment, significantly earlier than previously reported with this model (20). The Trask$^{+/+}$ control mice were euthanized at the same 12-week post-tamoxifen induction time point to enable a synchronous examination of histological sections in comparison with the Trask$^{-/-}$ mice. Tumor burden was quantitatively studied by the microscopic measurement of epidermal thickness as previously done (20). The epidermal thickness was on average 3.5 fold higher in Trask$^{-/-}$ SmoM2^{cond} K14-Cre^{ERT} mice compared with their Trask$^{+/+}$ counterparts ($p<0.0001$) (figure 3B, C and supplementary figure S3), indicating accelerated tumorigenesis in the absence of Trask function. Control mice from both Trask$^{+/+}$ and Trask$^{-/-}$ genotypes that were not treated with tamoxifen did not develop any gross skin disease or evidence of skin pathology on histologic sections (figure 3B, C).

Trask is not phosphorylated in the normal skin, but it is phosphorylated in the SmoM2-induced tumors (figure 3D). Both the normal skin and the skin tumors express only the uncleaved 140kD Trask form. We have previously described that the degree of cleavage of Trask varies considerably among cell types and its cleavage does not induce its phosphorylation (17–19).

Signaling in Trask null tumor cells

Immunoblot analysis of tumor lysates from several PyMT-driven mammary tumors revealed overall higher levels of MAPK signaling in the Trask$^{-/-}$ compared to the Trask$^{+/+}$ tumors (figure 4A), suggesting enhanced growth factor signaling in Trask$^{-/-}$ tumors as well as an overall increased level of FAK phosphorylation, consistent with the de-repression of integrin signaling in the absence of Trask. Receptor tyrosine kinome (RTK) profiling revealed that the predominant active RTK in these tumors is the HER family, specifically HER2 and to a lesser extent PDGFR (figure 4B) without much difference between the wildtype and Trask null tumors (data not shown). Primary tumor cell lines were generated from excised mammary tumors obtained from MMTV-PyMT, Trask$^{+/+}$ and MMTV-PyMT, Trask$^{-/-}$ mice. The *in vitro* proliferative growth of these tumors is dependent on growth factors. When grown in monolayer, there is no significant difference in the growth rates of the Trask$^{+/+}$ or Trask$^{-/-}$ tumor cells (figure 5A). However when grown in non-adhering plates, there is much higher spheroid formation in the Trask$^{-/-}$ compared with the Trask$^{+/+}$ tumor cells (figure 5B, C). In the Trask$^{+/+}$ genotype, these tumor cells form large spheroids with low efficiency, however in the Trask$^{-/-}$ genotype, spheroid formation is significantly enhanced with many more spheroids of all sizes evident. The phenotypic difference is specifically related to cell growth and not to cell-cell aggregation (supplementary figure S4).

We then studied differences in growth factor receptor signal transduction in the unanchored state. Our previous work had shown that Trask, when phosphorylated, inhibits integrin clustering and integrin outside-in signaling (9, 15–17). Since integrin signaling is known to cross-talk with RTK signaling, it is a logical next hypothesis that the phosphorylation of Trask, through its inhibition of integrin signaling, can inhibit integrin-RTK crosstalk, and

negatively impact RTK signaling (3–5). To test this hypothesis, we looked at RTK signaling in the Trask$^{+/+}$ and Trask$^{-/-}$ genotypes, and in the presence or absence of Trask phosphorylation. Trask phosphorylation by Src kinases is tightly linked with cell anchorage and is instantly induced upon loss of anchorage as previously described (11, 13, 15). Trask phosphorylation in PyMT-driven mammary tumor cells is similarly determined by their state of anchorage. In PyMT, Trask$^{+/+}$ tumor cells Trask is not phosphorylated when cultured in the adherent state (figure 5D, lane 1), but is phosphorylated if cultured in suspension (figure 5D, lane 2). Similarly, Trask is phosphorylated in tumor lysates from *in-vivo* growing mammary tumors from MMTV-PyMT Trask$^{+/+}$ mice (figure 5D, lane 3). Therefore when cultured *in vitro*, it is the anchorage-deprived state of these cells that mimicks their *in vivo* state, not their monolayer adherent state. When looking at growth factor signal transduction, we found that heregulin-driven signaling through MAPK is suppressed in suspended cells (figure 5E, compare lane 2 with 6). Trask is required for this detachment-specific suppression of MAPK signaling, since this suppression is not seen when Trask$^{-/-}$ tumor cells are deprived of anchorage (figure 5E, compare lane 4 with 8). There is a similar, although less pronounced suppression of Akt signaling in Trask$^{+/+}$ tumor cells which is also not seen in Trask$^{-/-}$ tumor cells.

The negative regulation of growth factor signaling does not appear to occur directly through the inhibition of RTK phosphorylation, since there is no difference in phosphorylation of HER2 or HER3 between Trask$^{+/+}$ and Trask $^{-/-}$ tumor cells (figure 6A). The negative effect is seen downstream of RTKs, such as in MAPK signaling. To interrogate whether this negative effect of Trask is specifically mediated through its inhibition of integrin signaling, we undertook experiments to manipulate integrin outside-in signaling both positively and negatively while in the unanchored state. To negatively impact integrin signaling we used the FAK inhibitor PF562271. As already shown above, heregulin-driven MAPK signaling is enhanced in Trask-null tumor cells (figure 6, compare lanes 2 with 4). This enhancement is mediated through FAK because it is not seen in cells treated with the FAK inhibitor PF562271 (figure 6, compare lanes 6 with 8). For positively impacting integrin signaling we used the integrin β1 antibody Ha2/5. This antibody interferes with the adhesion properties of integrin β1, but at the same time activates integrin β1 outside-in signaling (25, 26). Cell treated with the integrin β1 antibody Ha2/5 have enhancement of heregulin-driven MAPK signaling in Trask$^{+/+}$ tumor cells without any additional enhancement seen in Trask$^{-/-}$ cells (figure 6A, compare lanes 10 with 12). Thus the enhancement of RTK signaling seen in unanchored Trask-null tumor cells is due to loss of the integrin-suppressing functions of Trask manifested in the unanchored state, since it is recapitulated when integrin signaling is experimentally induced (by Ha2/5 antibody treatment), and it is overcome when integrin signaling is experimentally inhibited (by PF562271).

The activity of FAK, known to be linked with tumorigenic growth, is notably affected by the loss of Trask. This is most evident in the analysis of FAK inactivation during anchorage deprivation. When PyMT tumor cells are detached, FAK is dephosphorylated as expected (figure 6B, lanes 1,2). However this dephosphorylation is impaired in Trask$^{-/-}$ tumor cells leading to inappropriate FAK signaling despite the loss of anchorage (figure 6B, lanes 3,4). A similar effect can also be seen in human tumor cells through the shRNA knockdown of Trask (figure 6C). Therefore the loss of Trask function leads to constitutive and inappropriate FAK signaling, associated with enhancement of tumorigenic growth (27, 28).

The growth inhibitory functions of p-Trask appear to be a general mechanism that manifests during anchorage loss. To determine this, Trask was silenced in MCF10A non-transformed epithelial cells (figure 7A). When cultured in non-adherent plates, MCF10A cells form small spheroids with only very low efficiency, and mostly remain as single cells, or 2–3 cell aggregates. However the Trask knockdown cells show much more efficient spheroid

formation with significantly increased numbers of spheroids, increased size of spheroids, and increased total cell counts (determined through the analysis of viable cells in an MTT assay) when grown in anchorage-free conditions (figure 7B, C). MCF10A cells growing in matrigel typically grow into spherical forms of a limited size defined by a secreted basement membrane. Trask knockdown cells show enhanced growth with crowding of the central lumen and increased cell density and cell content of the spheroids, consistent with increased proliferative growth in the unanchored state (figure 7D, E). Anchorage loss was also studied *in vivo* using an experimental model of skin wounding. In skin wounding experiments, there is damage to tissue integrity surrounding the wound, leading to the phosphorylation of Trask in epithelial cells at the wound edge (supplementary figure S5) suggesting at least a partial impairment of cell anchorage and integrin signaling in these cells. When the wound repair process is histologically examined in the subsequent days, it appears that the epithelial layer at the wounded edge is thicker in $Trask^{-/-}$ mice compared with $Trask^{+/+}$ mice (supplementary figure S6). This is consistent with the *in vitro* experiments above which show a de-repression of growth in anchorage-impaired epithelial cells lacking Trask function.

Discussion

A major attribute of epithelial tumor cells is their ability to grow in an anchorage-independent manner. However the mechanisms that ordinarily restrict epithelial cell growth to the anchored state are not well defined. Here we define the phosphorylation of Trask as one such mechanism. Although in untransformed cells Trask is only phosphorylated when anchorage is lost (13), it is commonly phosphorylated in many areas of tumor tissues *in vivo*, consistent with a state of growth that is either fully or partially unanchored or at least defective in anchorage (18). While the fully or partially unanchored state of growth has advantages for tumorigenic growth, the phosphorylation of Trask in this state is a disadvantage, and therefore the loss of Trask enables tumors to grow much better in an anchorage-independent manner. The fact that the negative effects of Trask are much more significant in our *in vivo* models compared with the monolayer growth models is consistent with the fact that its tumor suppressing functions are manifest predominantly during the unanchored state. Consistent with this, we see a reduction or loss of Trask expression compared with the normal epithelium in many human cancers, including a survey of breast, colon, and prostate cancers (19, 29). The loss of Trask function in tumors may occur through allelic loss, as Trask resides on chromosome 3 at 3p21.3, an area associated with high frequency allelic loss in human cancers. The location of Trask between markers D3S1029 and D3S1478 place it within an area known to have loss of heterozygosity in a large fraction of lung cancer in a high resolution mapping effort (30, 31). Alternatively, the expression of Trask is lost in some tumors due to methylation silencing (19, 32). In a different mode of functional loss, Trask fails to undergo detachment-induced phosphorylation in some cancer cell lines (19). In our analysis of a panel of approximately 50 cancer cell lines, the cancer cell lines that expressed Trask but failed to phosphorylate it were all of the HER2-amplified subtype. This is entirely consistent with our findings that phosphorylated Trask interferes with integrin-growth factor receptor crosstalk, and previous studies showing that integrin signaling is particularly important in HER2-driven tumorigenesis (6, 7). In fact, HER2-driven tumor cells have been shown to be particularly dependent on integrin signaling during their unanchored state (33), creating unique pressure in this tumor type to eliminate the expression or phosphorylation of Trask.

In comparing PyMT tumor cell lines from the Trask wildtype or null background, it is apparent that growth factor receptor signaling is significantly enhanced in Trask null tumors. The enhancement is specifically seen in the unanchored state when Trask is phosphorylated and seems to suppress growth factor receptor signaling. The suppression of growth factor

signaling in the unanchored state is mediated through the inhibition of integrin signaling, since this suppression can be made redundant if FAK is directly inhibited, and it can be overcome if integrin β1 signaling is directly activated.

The fact that phosphorylated Trask inhibits integrin signaling is entirely consistent with the fact that it also inhibits growth factor signaling, since integrin signaling is well known to crosstalk with and enhance signaling from growth factor receptors (3, 4, 34, 35). Consistent with this, knockdown of β1 integrin diminishes EGFR signaling activity (36). How integrins facilitate growth factor receptor signaling is not yet clear. Integrins can be found in association with several growth factor receptors including EGFR and HER2 (37, 38). Integrins can induce ligand-independent activation of the EGF receptor or can synergistically enhance the growth factor induced activation of downstream MAPK without affecting receptor phosphorylation directly (35, 37). How integrins enhance growth factor receptor signaling is a subject of continuing debate. One proposed mechanism is that co-clustering with integrins creates increased local receptor density, promoting receptor dimerization and signaling. Another proposed mechanism is that co-localization with integrin clusters brings receptors into a subcellular micro-environment rich in signaling molecules, including various adaptor proteins, or second messengers including Src or FAK (reviewed in (3–5)). In our study of PyMT-driven tumors, we do not see an enhancement of HER2 or HER3 (or EGFR) phosphorylation in Trask null tumor cells, but we do see an enhancement in the activation of MAPK and to a lesser extent the activation of Akt. This is consistent with an effect of integrin signaling downstream of receptor phosphorylation in this tumor context. FAK itself has been proposed to mediate integrin-growth factor receptor crosstalk (39). Our data are also consistent with this as we see an attenuation of growth factor receptor signaling when cells are treated with FAK inhibitors. As seen in the PyMT-driven tumors *in vivo* and in culture, the loss of Trask leads to constitutive signaling by FAK, uncoupled from the state of anchorage. This by itself can enhance tumorigenic growth, as experimentally induced constitutive FAK signaling enhances tumorigenesis (28, 40).

Supplementary Material

Refer to Web version on PubMed Central for supplementary material.

Acknowledgments

Financial Support:

This work was funded by grant CA113952 (Moasser) from the National Institutes of Health. DS was supported by a Susan G. Komen for the Cure Postdoctoral fellowship and CHW was supported by a California Breast Cancer Research Program Postdoctoral fellowship. SYW was supported by NIH grant 1K99AR059796.

We wish to acknowledge the use of the Core Facilities of the Helen Diller Family Comprehensive Cancer Center, including the Gene Targeting core, the Mouse Pathology core, the Laboratory for Cell Analysis core, and the UCSF Sandler Lentiviral Core.

References

1. Goel HL, Languino LR. Integrin signaling in cancer. Cancer Treat Res. 2004; 119:15–31. [PubMed: 15164871]
2. Rathinam R, Alahari SK. Important role of integrins in the cancer biology. Cancer Metastasis Rev. 2010; 29:223–37. [PubMed: 20112053]
3. Alam N, Goel HL, Zarif MJ, Butterfield JE, Perkins HM, Sansoucy BG, et al. The integrin-growth factor receptor duet. J Cell Physiol. 2007; 213:649–53. [PubMed: 17886260]

4. Streuli CH, Akhtar N. Signal co-operation between integrins and other receptor systems. Biochem J. 2009; 418:491–506. [PubMed: 19228122]
5. Soung YH, Clifford JL, Chung J. Crosstalk between integrin and receptor tyrosine kinase signaling in breast carcinoma progression. BMB Rep. 2010; 43:311–8. [PubMed: 20510013]
6. Guo W, Pylayeva Y, Pepe A, Yoshioka T, Muller WJ, Inghirami G, et al. Beta 4 integrin amplifies ErbB2 signaling to promote mammary tumorigenesis. Cell. 2006; 126:489–502. [PubMed: 16901783]
7. Huck L, Pontier SM, Zuo DM, Muller WJ. beta1-integrin is dispensable for the induction of ErbB2 mammary tumors but plays a critical role in the metastatic phase of tumor progression. Proc Natl Acad Sci U S A. 2010; 107:15559–64. [PubMed: 20713705]
8. Scherl-Mostageer M, Sommergruber W, Abseher R, Hauptmann R, Ambros P, Schweifer N. Identification of a novel gene, CDCP1, overexpressed in human colorectal cancer. Oncogene. 2001; 20:4402–8. [PubMed: 11466621]
9. Bhatt AS, Erdjument-Bromage H, Tempst P, Craik CS, Moasser MM. Adhesion signaling by a novel mitotic substrate of src kinases. Oncogene. 2005; 24:5333–43. [PubMed: 16007225]
10. Hooper JD, Zijlstra A, Aimes RT, Liang H, Claassen GF, Tarin D, et al. Subtractive immunization using highly metastatic human tumor cells identifies SIMA135/CDCP1, a 135 kDa cell surface phosphorylated glycoprotein antigen. Oncogene. 2003; 22:1783–94. [PubMed: 12660814]
11. Brown TA, Yang TM, Zaitsevskaia T, Xia Y, Dunn CA, Sigle RO, et al. Adhesion or plasmin regulates tyrosine phosphorylation of a novel membrane glycoprotein p80/gp140/CUB domain-containing protein 1 in epithelia. J Biol Chem. 2004; 279:14772–83. [PubMed: 14739293]
12. He Y, Wortmann A, Burke LJ, Reid JC, Adams MN, Abdul-Jabbar I, et al. Proteolysis induced amino terminal ectodomain shedding of the integral membrane glycoprotein CUB domain containing protein 1 (CDCP1) is accompanied by tyrosine phosphorylation of its carboxy terminal domain and recruitment of Src and PKC{delta}. J Biol Chem. 2010
13. Spassov DS, Baehner FL, Wong CH, McDonough S, Moasser MM. The transmembrane src substrate Trask is an epithelial protein that signals during anchorage deprivation. Am J Pathol. 2009; 174:1756–65. [PubMed: 19349359]
14. Conze T, Lammers R, Kuci S, Scherl-Mostageer M, Schweifer N, Kanz L, et al. CDCP1 is a novel marker for hematopoietic stem cells. Ann N Y Acad Sci. 2003; 996:222–6. [PubMed: 12799299]
15. Spassov DS, Wong CH, Moasser MM. Trask phosphorylation defines the reverse mode of a phosphotyrosine signaling switch that underlies cell anchorage state. Cell Cycle. 2011; 10:1225–32. [PubMed: 21490433]
16. Spassov DS, Wong CH, Sergina N, Ahuja D, Fried M, Sheppard D, et al. Phosphorylation of Trask by Src kinases inhibits integrin clustering and functions in exclusion with focal adhesion signaling. Mol Cell Biol. 2011; 31:766–82. [PubMed: 21189288]
17. Spassov DS, Ahuja D, Wong CH, Moasser MM. The structural features of Trask that mediate its anti-adhesive functions. PLoS One. 2011; 6:e19154. [PubMed: 21559459]
18. Wong CH, Baehner FL, Spassov DS, Ahuja D, Wang D, Hann B, et al. Phosphorylation of the SRC epithelial substrate Trask is tightly regulated in normal epithelia but widespread in many human epithelial cancers. Clin Cancer Res. 2009; 15:2311–22. [PubMed: 19318475]
19. Spassov DS, Wong CH, Harris G, McDonough S, Phojanakong P, Wang D, et al. A tumor-suppressing function in the epithelial adhesion protein Trask. Oncogene. 2011
20. Wong SY, Seol AD, So P-L, Ermilov AN, Bichakjian CK, Epstein EH, et al. Primary cilia can both mediate and suppress Hedgehog pathway-dependent tumorigenesis. Nature medicine. 2009; 15:1055–61.
21. Chmielowiec J, Borowiak M, Morkel M, Stradal T, Munz B, Werner S, et al. c-Met is essential for wound healing in the skin. J Cell Biol. 2007; 177:151–62. [PubMed: 17403932]
22. Romer J, Bugge TH, Pyke C, Lund LR, Flick MJ, Degen JL, et al. Impaired wound healing in mice with a disrupted plasminogen gene. Nature medicine. 1996; 2:287–92.
23. Debnath J, Muthuswamy SK, Brugge JS. Morphogenesis and oncogenesis of MCF-10A mammary epithelial acini grown in three-dimensional basement membrane cultures. Methods. 2003; 30:256–68. [PubMed: 12798140]

24. Guy CT, Cardiff RD, Muller WJ. Induction of mammary tumors by expression of polyomavirus middle T oncogene: a transgenic mouse model for metastatic disease. Molecular and Cellular Biology. 1992; 12:954–61. [PubMed: 1312220]
25. Armulik A, Velling T, Johansson S. The integrin beta1 subunit transmembrane domain regulates phosphatidylinositol 3-kinase-dependent tyrosine phosphorylation of Crk-associated substrate. Mol Biol Cell. 2004; 15:2558–67. [PubMed: 15034138]
26. Wennerberg K, Fassler R, Warmegard B, Johansson S. Mutational analysis of the potential phosphorylation sites in the cytoplasmic domain of integrin beta1A. Requirement for threonines 788–789 in receptor activation. J Cell Sci. 1998; 111 (Pt 8):1117–26. [PubMed: 9512507]
27. Lahlou H, Sanguin-Gendreau V, Zuo D, Cardiff RD, McLean GW, Frame MC, et al. Mammary epithelial-specific disruption of the focal adhesion kinase blocks mammary tumor progression. Proc Natl Acad Sci U S A. 2007; 104:20302–7. [PubMed: 18056629]
28. Pylayeva Y, Gillen KM, Gerald W, Beggs HE, Reichardt LF, Giancotti FG. Ras- and PI3K-dependent breast tumorigenesis in mice and humans requires focal adhesion kinase signaling. J Clin Invest. 2009; 119:252–66. [PubMed: 19147981]
29. Siva AC, Wild MA, Kirkland RE, Nolan MJ, Lin B, Maruyama T, et al. Targeting CUB domain-containing protein 1 with a monoclonal antibody inhibits metastasis in a prostate cancer model. Cancer Res. 2008; 68:3759–66. [PubMed: 18483259]
30. Ji L, Minna JD, Roth JA. 3p21.3 tumor suppressor cluster: prospects for translational applications. Future Oncol. 2005; 1:79–92. [PubMed: 16555978]
31. Wistuba II, Behrens C, Virmani AK, Mele G, Milchgrub S, Girard L, et al. High resolution chromosome 3p allelotyping of human lung cancer and preneoplastic/preinvasive bronchial epithelium reveals multiple, discontinuous sites of 3p allele loss and three regions of frequent breakpoints. Cancer Res. 2000; 60:1949–60. [PubMed: 10766185]
32. Ikeda JI, Morii E, Kimura H, Tomita Y, Takakuwa T, Hasegawa JI, et al. Epigenetic regulation of the expression of the novel stem cell marker CDCP1 in cancer cells. J Pathol. 2006; 210:75–84. [PubMed: 16823897]
33. Jenndahl LE, Taylor-Papadimitriou J, Baeckstrom D. Characterization of integrin and anchorage dependence in mammary epithelial cells following c-erbB2-induced epithelial-mesenchymal transition. Tumour Biol. 2006; 27:50–8. [PubMed: 16340250]
34. Aplin AE, Juliano RL. Integrin and cytoskeletal regulation of growth factor signaling to the MAP kinase pathway. J Cell Sci. 1999; 112 (Pt 5):695–706. [PubMed: 9973604]
35. Miyamoto S, Teramoto H, Gutkind JS, Yamada KM. Integrins can collaborate with growth factors for phosphorylation of receptor tyrosine kinases and MAP kinase activation: roles of integrin aggregation and occupancy of receptors. J Cell Biol. 1996; 135:1633–42. [PubMed: 8978828]
36. Morello V, Cabodi S, Sigismund S, Camacho-Leal MP, Repetto D, Volante M, et al. [beta]1 integrin controls EGFR signaling and tumorigenic properties of lung cancer cells. Oncogene. 2011; 30:4087–96. [PubMed: 21478906]
37. Moro L, Dolce L, Cabodi S, Bergatto E, Boeri Erba E, Smeriglio M, et al. Integrin-induced epidermal growth factor (EGF) receptor activation requires c-Src and p130Cas and leads to phosphorylation of specific EGF receptor tyrosines. J Biol Chem. 2002; 277:9405–14. [PubMed: 11756413]
38. Falcioni R, Antonini A, Nistico P, Di Stefano S, Crescenzi M, Natali PG, et al. Alpha 6 beta 4 and alpha 6 beta 1 integrins associate with ErbB-2 in human carcinoma cell lines. Exp Cell Res. 1997; 236:76–85. [PubMed: 9344587]
39. Renshaw MW, Price LS, Schwartz MA. Focal adhesion kinase mediates the integrin signaling requirement for growth factor activation of MAP kinase. J Cell Biol. 1999; 147:611–8. [PubMed: 10545504]
40. Frisch SM, Vuori K, Ruoslahti E, Chan-Hui PY. Control of adhesion-dependent cell survival by focal adhesion kinase. J Cell Biol. 1996; 134:793–9. [PubMed: 8707856]

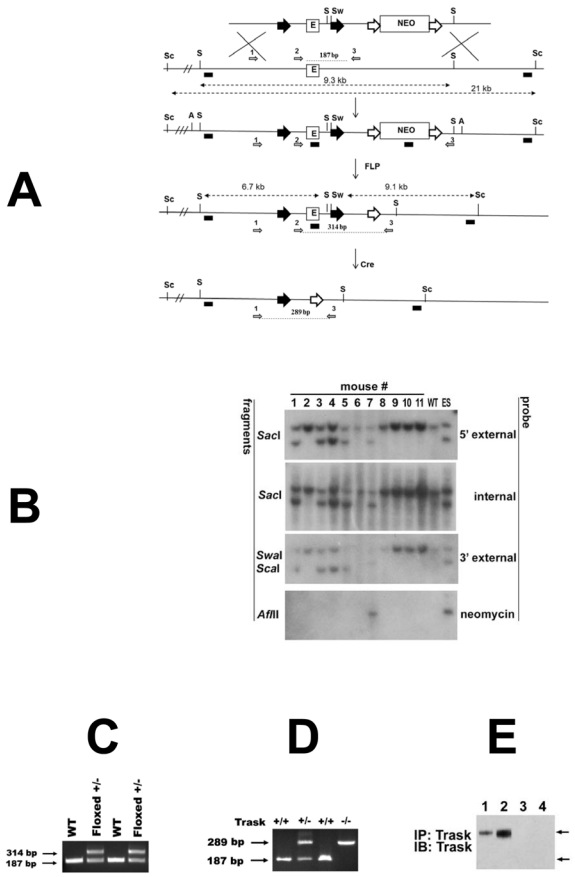

Figure 1. Targeting of the murine Trask locus

(A) Diagrams of the targeted locus and construct used for the generation of Trask floxed and null mice. The loxp sites are shown as big black arrowheads that flank 1.4 kb fragment containing exon 1 (E) and core promoter sequences (not shown). Neomycin cassette (Neo) is flanked by FRT sites (big white arrows). The SacI (S), SwaI (Sw), Sca1 (Sc) and AflII (A) restriction site used for Southern analysis are indicated. The probes used for analysis include 5′ external, internal (exon1), 3′ external and Neo are depicted as small black boxes. The diagnostic SacI and Sca-1 SwaI fragments are shown with punctuated lines with double arrowheads. The removal of the Neo was achieved by crossing with actin-FLP mice, and generation of the null allele by crossing with EIIa-Cre transgenic mice. The PCR primers used for genotyping of floxed and null mice are depicted as small grey arrows and numbered 1, 2 and 3. (B) Southern analysis for germline transmission and Neo excision. Genomic DNA from the progeny of Trask chimeric mice and actin-FLP mice were digested with the indicated restriction enzymes and analyzed with 5′ extrenal, internal, 3′ external and Neo probes. DNA from wild type (WT) mouse and targeted ES clone were used as controls. Mice 1, 3, 4, and 5 are floxed $^{+/-}$ and used as founders for subsequent crossing. (C) Genotyping with primers 2 and 3 gives 187 bp product from the wt template and 314 bp product from the floxed allele. (D) PCR analysis of tail DNA with primers 1,2 and 3 were used to genotype Trask $^{+/+}$, Trask $^{+/-}$ and Trask $^{-/-}$ mice. (E) The expression of Trask protein was assayed by immunoprecipitation and immunoblotting of lysates in mouse skin (1,3) and intestine (2,4) in Trask $^{+/+}$ (1,2) and Trask $^{-/-}$ (3,4) mice. Only the 140 kD Trask is expressed in these mouse tissues.

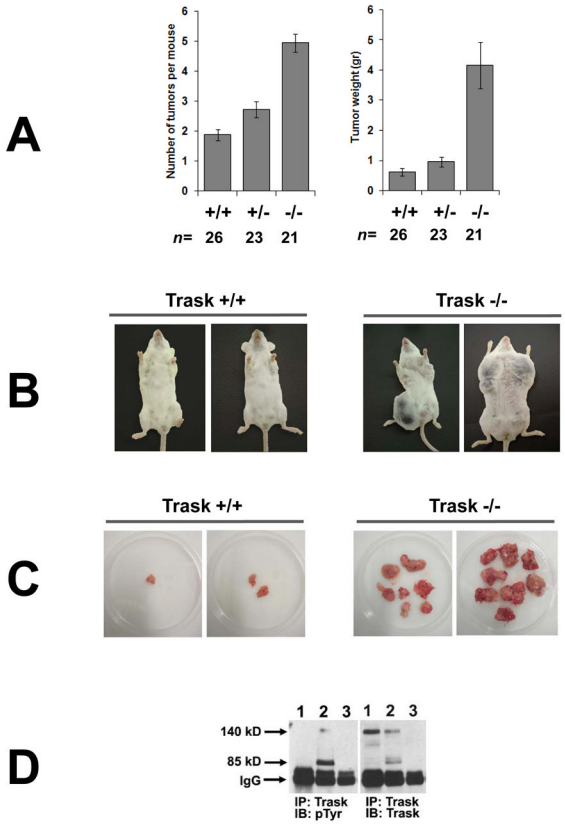

Figure 2. Inactivation of Trask accelerates PyMT induced tumorigenesis

(A) Mammary tumorigenesis in mice carrying an MMTV-PyMT transgene was compared among mice carrying the indicated Trask genotypes. Trask $^{-/-}$ mice have both an increase in the number of detectable tumors and in the weight of the tumors. The difference between +/+ and −/− genotypes is highly significant in both tumor number ($p<0.001$) and tumor weight ($p<0.001$). The difference between +/+ and +/− genotypes is more modest, but also significant in both tumor number ($p<0.005$) and tumor weight ($p<0.04$). (B) Pictures of representative age-matched tumor-bearing mice are shown for the Trask$^{+/+}$ (left) and Trask $^{-/-}$ (right) genotypes.

(C) Representative *ex vivo* images of PyMT mammary tumors from Trask $^{+/+}$ and Trask$^{-/-}$ mice. Each dish contains the entire tumor burden of a single mouse. Trask null mice have both an increase in the number of tumors and in the size of the tumors. (D) Lysates from mouse tissue were assayed by immunoprecipitation. Lanes correspond to 1) normal mammary gland from Trask $^{+/+}$ mouse, 2) mammary tumor from PyMT, Trask $^{+/+}$ mouse, 3) mammary tumor from MMTV-PymT, Trask $^{-/-}$ mouse. Trask is phosphorylated in PyMT tumors, but not in the normal mouse mammary gland.

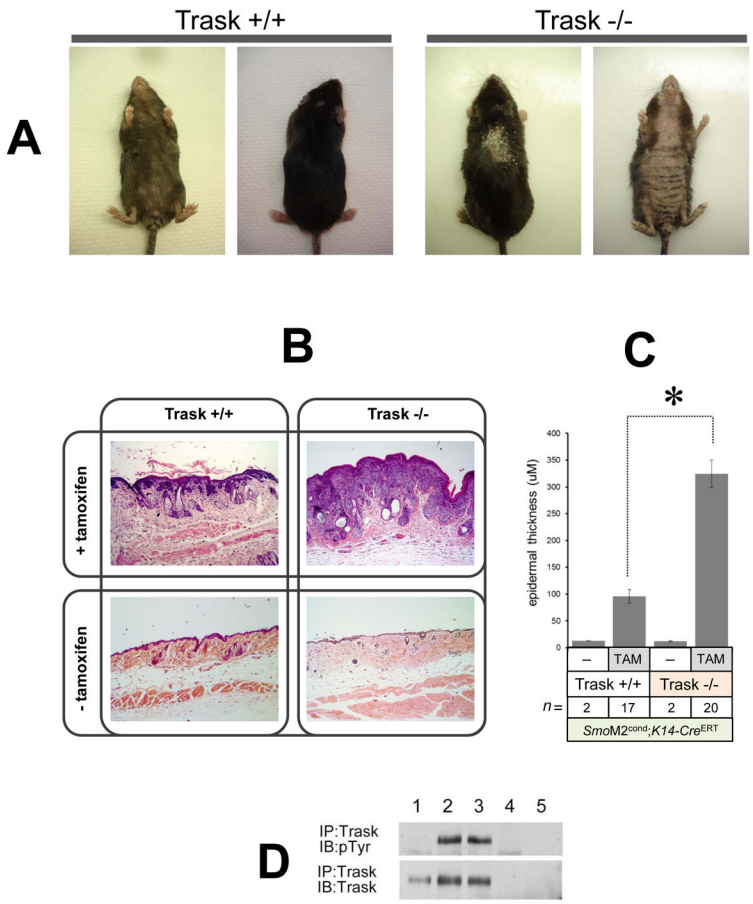

Figure 3. Inactivation of Trask accelerates SmoM2 induced neoplasia

(A) Conditional SmoM2 mice in the indicated Trask genotypes were treated with tamoxifen to induce the oncogenic SmoM2 allele. Dorsal and abdominal view of representative Trask $^{+/+}$ (left) and Trask $^{-/-}$ (right) mice are shown 12 weeks after tamoxifen treatment. Note more severe hair loss, scaling and skin thickening in Trask null mice. (B) Representative H&E staining of skin samples from K14-Cre^{ERT} SmoM2 Trask $^{+/+}$ and K14-Cre^{ERT} SmoM2 Trask $^{-/-}$ mice treated with or without tamoxifen. Skin samples were taken 12 weeks after tamoxifen injection.

(C) Quantification of epidermal thickness (reflecting tumor burden) from histopathology sections showing much thicker tumors in the Trask $^{-/-}$ mice ($p<0.0001$). This analysis was performed on 17 K14-Cre^{ERT} SmoM2 Trask $^{+/+}$ and 20 K14-Cre^{ERT} SmoM2 Trask $^{-/-}$ mice 12 weeks after tamoxifen treatment. Control mice were not injected with tamoxifen. (D) The expression and phosphorylation of Trask was assayed as indicated from mouse skin by immunoprecipitation. Lanes correspond to 1) normal mouse skin, 2,3) skin from two Trask $^{+/+}$ mice bearing SmoM2-induced skin tumors, 4) skin from a Trask $^{-/-}$ mouse bearing an SmoM2-induced skin tumor, 5) IgG immunprecipitate from a tumor-bearing Trask $^{+/+}$ mouse skin. The mouse skin and SmoM2 induced tumors express only the full-length 140 kD Trask form. Trask is phosphorylated in SmoM2 induced tumors, but not in the normal mouse skin.

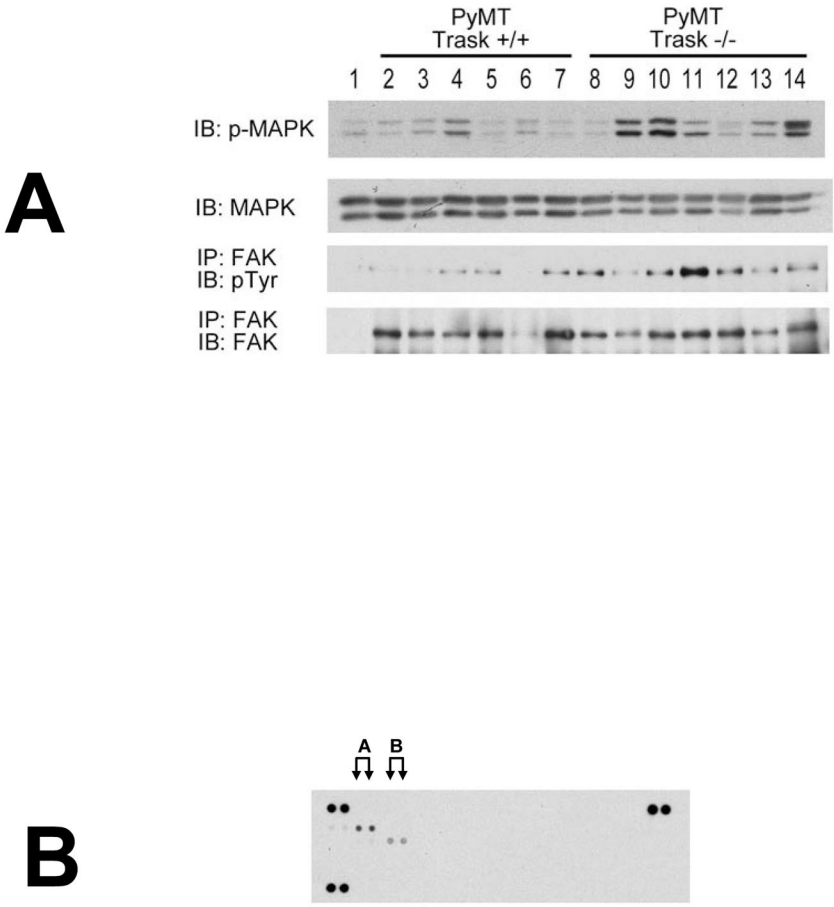

Figure 4. Integrin and growth factor signaling in PyMT tumors *in vivo*

(A) Lysates from PyMT Trask $^{+/+}$ and PyMT Trask $^{-/-}$ tumors were analyzed by immunoblotting. Phosphorylation of MAPK (T202/Y204), tyrosine phosphorylation of FAK and their total protein expressions are shown. Each lane corresponds to a tumor derived from a different mouse. (B) The Trask $^{+/+}$ tumor lysates were used in the R&D Systems p-RTK profiling. This analysis revealed that the predominant active RTK in these tumors is HER2 (labeled A) and to a lesser extent PDGFR (labeled B).

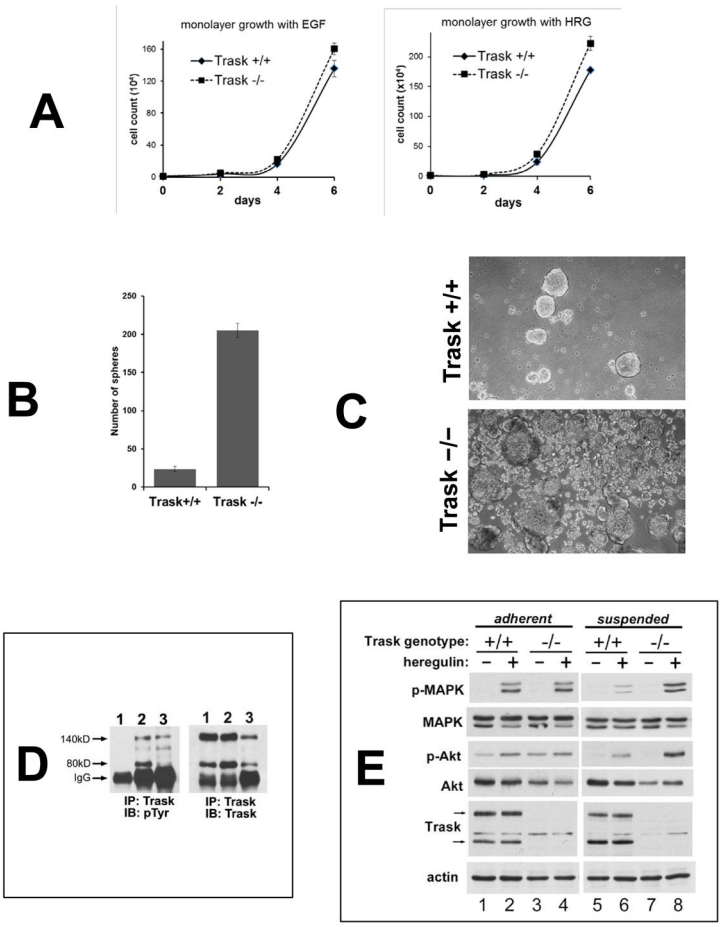

Figure 5. Loss of Trask augments growth factor signaling in PyMT tumor derived cell lines

(A) Tumor cell lines from MMTV-PyMT mice in the indicated Trask genotypes were grown in the presence of either epidermal growth factor or heregulin for six days and counted. (B) Tumor cell lines from PyMT-driven mouse mammary tumors originating from Trask$^{+/+}$ or Trask$^{-/-}$ mice were cultured in non-adherent plates for 7 days and the number of spheroids counted manually under microscopic examination. (C) Phase contrast microscope images of the spheroids are shown here. (D) Cell lysates were assayed for the expression and phosphorylation of Trask by immunoprecipitation. Lanes correspond to 1) PyMT tumor cell line cultured in the adherent state, 2) PyMT tumor cell line cultured in the suspended state, 3) *in vivo* PyMT tumor from a mouse. Trask is phosphorylated during tumor growth *in vivo*, resembling the suspended state when grown in culture. (E) Serum starved PyMT cell lines from the indicated genotypes were grown in adherent or suspended form were stimulated with heregulin. The growth factor-induced activation of MAPK is suppressed in the suspended Trask$^{+/+}$ cells. This suppression does not occur in Trask$^{-/-}$ cells. There is a more subtle enhancement of Akt signaling in the Trask$^{-/-}$ cells. The arrows indicate the 140 and 80kD forms of Trask. The phospho-immunoblots reflect the T202/Y204 phosphorylation of MAPK and the S473 phosphorylation of Akt.

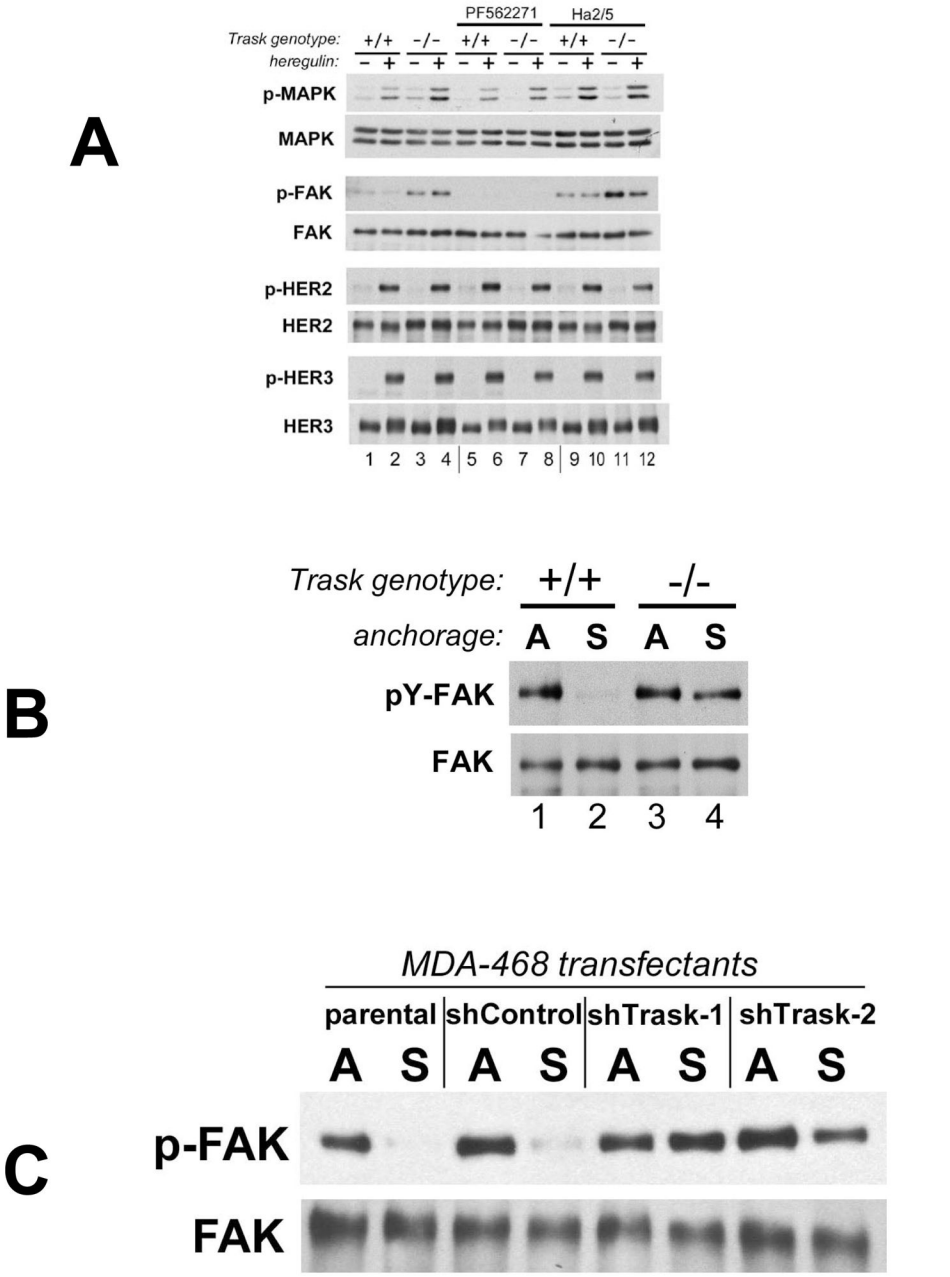

Figure 6. Trask inhibits integrin signaling and disrupts integrin-growth factor receptor crosstalk

(A) PyMT cell lines were serum starved for 24 hrs, detached and incubated in suspended conditions. Cells were incubated with FAK inhibitor PF562271 or β1-integrin activating antibody Ha2/5 for 2 hrs, followed by stimulation with herugulin for 10 min as indicated. Phosphorylation of MAPK (T202/Y204), FAK (all tyrosines), HER2 (Y1248) and HER3 (Y1289) and their total expression levels was determined by immunoblotting. (B) PyMT tumor cell lines from Trask $^{+/+}$ and $^{-/-}$ mice were assayed while adherent (A), or after 2 hours of culture in suspension in non-adhering plates (S). The phosphorylation state of FAK was assayed by IP/pTyr analysis. FAK is normally dephosphorylated when anchorage is lost (lane 2). But in Trask $^{-/-}$ cells, there is abnormal persistence of FAK phosphorylation in the unanchored state (lane 4). (C) The same analysis was done in MDA-468 breast cancer cells

looking at p-FAK in suspension using either of two Trask shRNA knockdown pools compared with control cells (parental or non-silencing shRNA transfectant).

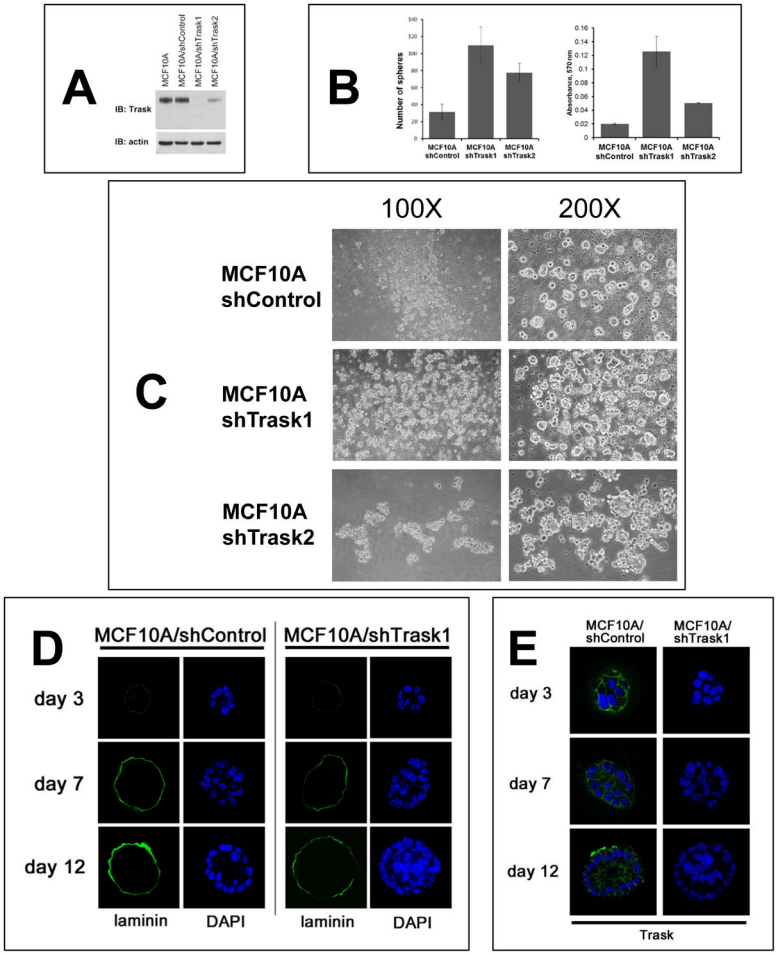

Figure 7. Anchorage-independent growth in the presence or absence of Trask

(A) MCF10A cells were engineered to stably express either of two Trask-targeting shRNAs or a non-silencing shRNA and the loss of Trask expression in these cells was confirmed by immunoblotting. MCF10A/shTrask1 cells have a complete loss of Trask while MCF10A/shTrask2 cells have a partial loss of Trask expression. (B) The indicated cell types were cultured in non-adherent plates for 6 days and the number of spheroids counted manually by microscopic examination in triplicate wells (left). The total number of cells in each well was also compared using the MTT assay (right). (C) The appearance of the spheroids was captured by phase contrast microscopy at the indicated magnifications for the three cell types. (D) MCF10A/shControl and MCF10A/shTrask1 cells were grown on matrigel for the indicated number of days and the cellular architecture, density, and expression of laminin were determined by immunofluorescence staining and confocal microscopy. Laminin was stained using green-fluorescent reagents and DAPI staining was used to stain the cell nuclei. (E) Additional sections were stained with anti-Trask antibodies in green as shown.